

Revealing Optically Induced Magnetization in SrTiO_3 using Optically Coupled SQUID Magnetometry and Magnetic Circular Dichroism

W. D. Rice,¹ P. Ambwani,² J. D. Thompson,³ C. Leighton,² and S. A. Crooker¹

¹*National High Magnetic Field Laboratory, Los Alamos National Laboratory, Los Alamos, NM 87545, USA*

²*Department of Chemical Engineering and Materials Science,
University of Minnesota, Minneapolis, MN 55455, USA*

³*Materials Physics and Applications Division, Los Alamos National Laboratory, Los Alamos, NM 87545, USA*

(Dated: March 2, 2022)

In this work, we study the time- and temperature-dependence of optically induced magnetization in bulk crystals of slightly oxygen-deficient $\text{SrTiO}_{3-\delta}$ using an optically coupled SQUID magnetometer. We find that a weak ($\sim 5 \times 10^{-7}$ emu) but extremely long-lived (hours) magnetic moment can be induced in $\text{SrTiO}_{3-\delta}$ at zero magnetic field by circular-polarized sub-bandgap light. We utilize this effect to demonstrate that $\text{SrTiO}_{3-\delta}$ crystals can be used as an optically addressable magnetic memory by writing and subsequently reading magnetic patterns with light. The induced magnetization is consistent with that of a polarized ensemble of independent oxygen-vacancy-related complexes, rather than from collective or long-range magnetic order.

The developing field of complex oxide electronics is intimately tied to its most widely studied member, strontium titanate (SrTiO_3)^{1–5}. While the electronic and optical properties of bulk SrTiO_3 have been thoroughly investigated^{6–9}, SrTiO_3 has recently drawn renewed research interest mainly driven by the discovery of magnetism and superconductivity at epitaxial interfaces between SrTiO_3 and other complex oxides^{5,10–16}. Because oxygen vacancies, V_O , are easily formed in SrTiO_3 and act as electron donors, it has been widely conjectured that V_O may play a key role in these emergent electronic and magnetic phenomena^{17–21}. Interest in nominally non-magnetic bulk SrTiO_3 has been further fueled by observations of the Kondo effect and magnetization in ionically gated SrTiO_3 crystals²².

Recently we reported²³ the observation of persistent optically induced magnetization in bulk crystals of slightly oxygen-deficient $\text{SrTiO}_{3-\delta}$. Specifically, circularly polarized light at sub-bandgap wavelengths between 400 nm and 500 nm was found to induce a magnetic moment (in zero magnetic field) that persisted from seconds at ~ 18 K to several hours below 10 K. This magnetization was attributed to a partial spin polarization within the ground state of local V_O -related complexes. While these effects were investigated primarily using magnetic circular dichroism (MCD) spectroscopy, critical time- and temperature-dependent behaviors were directly confirmed using a variant of conventional SQUID magnetometry²³. Moreover, it was demonstrated that detailed spatial magnetic patterns could be written into and read from $\text{SrTiO}_{3-\delta}$ using light alone.

The primary intent of this paper is therefore to provide details of the optically coupled SQUID magnetometry technique that was utilized to confirm the presence of optically induced magnetization in our $\text{SrTiO}_{3-\delta}$ crystals, and also to fully describe the MCD-based optical system that was used to write and read magnetic patterns in $\text{SrTiO}_{3-\delta}$. Detailed experimental schematics are shown, along with data that further support a scenario in which

the induced magnetic moment arises *not* from long-range or collective magnetic order, but rather (and more simply) from a long-lived spin polarization within an ensemble of localized and independent V_O -related complexes.

In these studies, nominally pure 500 μm thick SrTiO_3 (100) crystals from MTI Corporation were annealed in ultra-high vacuum (oxygen partial pressure $< 10^{-9}$ Torr) at temperatures between 650–750°C, conditions that promote diffusion of oxygen out of the lattice²⁴. This annealing (*i.e.*, reduction) treatment was used to make a set of nine slightly oxygen-deficient $\text{SrTiO}_{3-\delta}$ crystals with varying V_O densities. To measure the V_O density, we soldered indium contacts to the corners of each sample in a van der Pauw geometry and measured the electron concentration, n , using longitudinal resistivity and/or Hall-effect transport studies. Assuming that every V_O contributes one to two electrons to the conduction band (in the simplest models), the approximate V_O concentration can be inferred from n . In this work, n ranged from $\sim 10^{14} \text{ cm}^{-3}$ to $8 \times 10^{17} \text{ cm}^{-3}$.

In our previous work²³, optically induced magnetization in these $\text{SrTiO}_{3-\delta}$ crystals was studied primarily via the technique of MCD spectroscopy. While non-zero MCD signals typically imply the presence of time-reversal breaking (*e.g.*, magnetism)²⁵, we felt that it was important to independently confirm magnetism in our $\text{SrTiO}_{3-\delta}$ crystals using a *direct* SQUID-based probe of the optically induced magnetic moment. Besides providing a quantitative measure of the induced moment, SQUID magnetometry also avoids certain artifacts (such as material gyrotropism) that can, in certain circumstances, generate MCD or Kerr-effect signals that are not related to real magnetism²⁶.

To this end, we sought to perform SQUID magnetometry on our $\text{SrTiO}_{3-\delta}$ crystals while illuminating the crystals with light whose *optical polarization* could be established and controlled – *in situ* – with a high degree of fidelity and precision. While many commercial SQUID systems provide options allowing samples to be illumi-

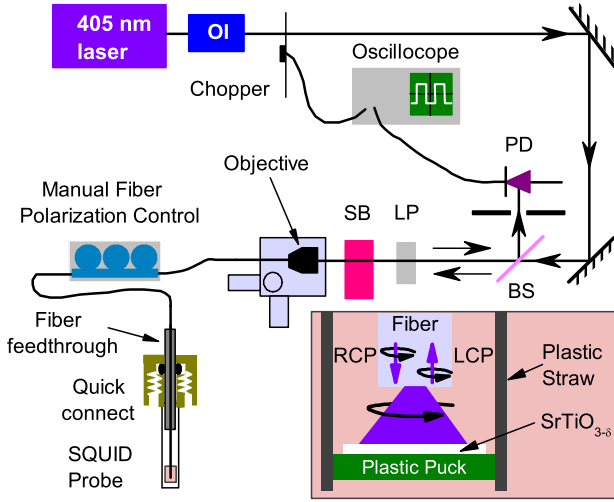


FIG. 1. Optically coupled SQUID magnetometry. Mechanically chopped 405 nm light from a laser diode is passed through an optical isolator (OI) and is circularly polarized by a linear polarizer (LP) and Soleil-Babinet compensator (SB) before being coupled into a standard UV single-mode fiber. The light that is back-reflected from the other end of the fiber (in the SQUID magnetometer) follows a time-reversed path back through the fiber, SB, and LP and is directed to a photodiode (PD) using a beamsplitter (BS). Its intensity is zero (it is completely nulled by LP) if the optical polarization at the *end* of the fiber is exactly LCP or RCP. A manual fiber polarization controller allows to compensate for unwanted strain-induced birefringence in the fiber in order to maintain circular polarization at the sample. Inset: Detailed view of fiber end near sample. The sample is mounted on a plastic Kel-F (polychlorotrifluoroethylene) puck that is held by friction in a plastic straw.

nated, this is typically achieved via multi-mode optical fibers that scramble the polarization of the transmitted light. Therefore we constructed a portable optical setup based on polarization control within a standard single-mode fiber (SMF). Although bends and strain in a SMF generate birefringence that can alter the polarization state of light traveling within the SMF, the output polarization of the light is not irretrievably scrambled. Rather, it has a definite and measurable relationship to the input polarization, because the light travels only along a single optical mode. Importantly, any undesired birefringence or polarization changes in the SMF can be compensated and “undone” by carefully and intentionally straining the SMF using a manual fiber polarization controller. Related fiber-based approaches to couple polarized light to SQUID magnetometers have been used in the past to study, for example, magnetic polarons in diluted magnetic semiconductors²⁷.

Figure 1 depicts the optical setup that we used in conjunction with a commercial Quantum Design MPMS SQUID magnetometer. The system uses a standard probe whose top was modified to admit a single-mode optical fiber (here, the bare fiber was stripped of its plas-

tic jacket and epoxied into a 10 cm length of brass tubing, that was in turn fed through a standard vacuum quick-connect). The fiber emanating from the probe to the optical setup was carefully suspended far above the fiber feedthrough to minimize any strain or twisting of the fiber when the SQUID probe translates vertically during measurements; in doing so we find that the optical polarization is unaffected. Optical polarization conditioning and monitoring was achieved with components on a portable 300 mm × 600 mm optical breadboard that was located near the SQUID. Circularly polarized 405 nm laser light was coupled into a standard UV bare SMF using an aspheric objective lens and a fiber launcher with piezoelectric actuators. Free-space circular polarization was produced before the fiber using a linear polarizer (LP) and a Soleil-Babinet compensator (SB) on a rotational mount. To compensate for unwanted birefringence in the SMF due to bending and strain, we threaded the fiber through a three-paddle fiber polarizer controller.

To infer the polarization state of the light at the sample, we monitored the light that was back-reflected from the other end of the fiber (in the SQUID, just above the sample). This back-reflected light travels a time-reversed path back through the optical system (fiber, SB, and LP), where it is picked off using a beamsplitter and measured with a photodiode (PD) and oscilloscope. Mechanically chopping the beam provides a convenient baseline determination on the oscilloscope trace.

The crucial point is that the back-reflected light will be polarized exactly orthogonal to the linear polarizer LP (giving zero intensity at the photodiode) *only* when the light at the end of the fiber – and therefore at the sample – is circularly polarized (because only circular polarized light exactly reverses its helicity upon reflection). Thus, manually straining the fiber to compensate for any unwanted birefringence in the SMF and zeroing the back-reflected intensity at the photodiode guarantees circularly polarized light at the sample. Once one sense of circularly polarized light is obtained, rotating the Soleil-Babinet compensator by 45 or 90 degrees produces linear or oppositely circularly polarized light at the sample, respectively (and a corresponding maximum and second minimum of the back-reflected intensity). As might be expected, any significant movement or bending of the fiber during an experiment requires a re-adjustment and balancing of the manual polarization controller. This setup therefore utilizes the back-reflected intensity as a continuous and *in situ* monitor of the optical polarization at the sample in the SQUID.

We used the optically coupled SQUID magnetometer to perform both time- and temperature-dependent magnetometry on oxygen-deficient $\text{SrTiO}_{3-\delta}$ crystals and also on unannealed (as-received) SrTiO_3 . Typical sample sizes were approximately 3 mm × 3 mm × 0.5 mm with measurements of the magnetic moment being collected roughly every 90 seconds in zero magnetic field with an average illumination power of $\sim 200 \mu\text{W}$. Figure 2(a) dis-

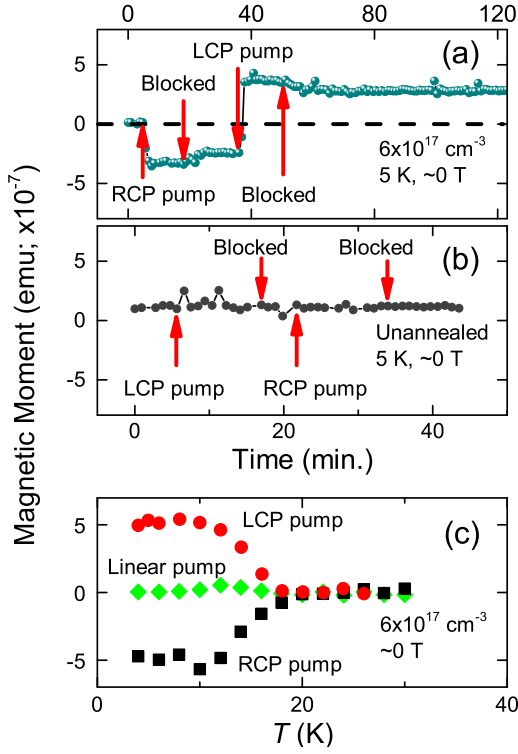


FIG. 2. (a) The temporal evolution of the optically induced magnetic moment in $\text{SrTiO}_{3-\delta}$, as measured by the optically coupled SQUID, shows that magnetization at 5 K is maintained for hours even after the light has been blocked. RCP and LCP light induce equal, but opposite, magnetic moments. (b) No optically induced magnetic moment is observed when the V_O density is very low, as in unannealed SrTiO_3 . (c) Temperature-dependent optically induced magnetic moment for RCP (black), LCP (red), and linearly (green) polarized pumping as measured by SQUID magnetometry (adapted from Rice *et al.*²³, with permission from Nature Publishing Group).

plays how the magnetic moment evolves during and after pumping with circularly polarized light. For both RCP and LCP light, the magnitude of the optically induced magnetic moment is $\sim 5 \times 10^{-7} \text{ emu}$, with RCP and LCP light creating equal but oppositely-oriented magnetic moments. At low temperatures, the magnetization persists for over an hour even after the light is blocked, in agreement with MCD results²³. To ensure that only samples with oxygen vacancies produced this effect, we also tested an unannealed (as-received) SrTiO_3 crystal under the same conditions. As seen in Fig. 2(b), no magnetic moment is induced regardless of the polarization of light. The slight offset in the measured magnetic moment is likely due to the small remnant magnetic field of the superconducting magnet ($\sim 10^{-4} \text{ T}$) and the intrinsic diamagnetism of the sample and the plastic puck on which it was mounted.

Temperature-dependent magnetization for RCP, LCP, and linearly polarized illumination was also investigated. As shown in Fig. 2(c), the optically induced magnetic

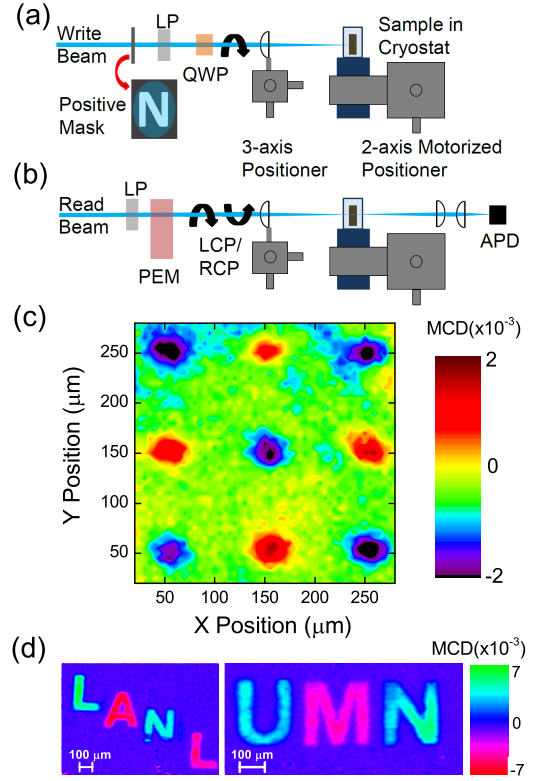


FIG. 3. (a) Experimental configuration used to optically write magnetic images in $\text{SrTiO}_{3-\delta}$ at zero field. A linear polarizer (LP) and quarter-wave plate (QWP) are used to create RCP or LCP light that can be imaged onto the sample through a positive mask. (b) Setup used to optically read magnetic images using raster-scanned MCD. A photo-elastic modulator (PEM) produces alternating RCP/LCP light that is transmitted through the sample and detected by an avalanche photodiode (APD). (c,d) 2-D images of detected magnetic patterns in $\text{SrTiO}_{3-\delta}$; here, the magnetization is reversed at each subsequent dot/letter (Fig. 3d adapted from Rice *et al.*²³, with permission from Nature Publishing Group).

moment $M(T)$ undergoes a steep increase below 18 K when continuously pumped with either RCP or LCP light; however, no net magnetization is observed for linearly polarized illumination. Again, RCP and LCP light induce equal and opposite magnetic moments. M saturates when T decreases below $\sim 10 \text{ K}$, a behavior that agrees well with MCD studies²³, and which is shown below to be independent of the V_O density.

Optically producing a long-lived magnetic moment in zero applied magnetic field is a potentially exciting development both scientifically and technologically. Figure 3 demonstrates that $\text{SrTiO}_{3-\delta}$ can potentially be utilized as a component in an optically-addressable magnetic memory device. We created an imaging system that can optically write and read spatial magnetic patterns in $\text{SrTiO}_{3-\delta}$ [Fig. 3(a,b)]. For this demonstration, we detected either simple magnetic “dots” or more complex magnetic patterns that were written with 400 nm LCP/RCP light [Figs. 3(c,d)]. Writing was typically ac-

complished by passing RCP or LCP light through a positive mask and imaging it on to a $\text{SrTiO}_{3-\delta}$ crystal at low temperature. To read these magnetic patterns, a raster-scanned optical MCD probe was used to measure magnetization as a function of position.

MCD spectroscopy is an all-optical technique that measures the normalized difference between transmission (T) of RCP and LCP light: $\text{MCD} \propto \frac{T_{\text{RCP}} - T_{\text{LCP}}}{T_{\text{RCP}} + T_{\text{LCP}}}$. Non-zero MCD signals are usually attributed to broken time-reversal symmetry (*e.g.*, magnetism) and can be used to study a wide variety of magneto-optical phenomena²⁵. A key benefit of MCD methods over conventional (SQUID, for example) magnetometry is its detailed spectral dependence, which provides information on the energies of polarizable and magneto-optically active states. As previously shown²³, optically induced magnetization in $\text{SrTiO}_{3-\delta}$ is most clearly revealed in the wavelength range between 400-500 nm (just below the band edge), with a particularly strong response at 425 nm. Therefore in the MCD images shown here, probe light at 425 nm was modulated between RCP and LCP at 50 kHz by a photo-elastic modulator (PEM) and was mechanically chopped at 137 Hz to facilitate lock-in detection of $T_{\text{RCP}} - T_{\text{LCP}}$ and $T_{\text{RCP}} + T_{\text{LCP}}$, respectively. This probe light was focused and raster-scanned across the sample to construct a two-dimensional image of magnetization. In these experiments, the minimum size of the magnetic patterns was effectively limited by the large thickness of the samples; we selected optics for which the Rayleigh range of focused pump and probe light was commensurate with the 500 μm thickness of the $\text{SrTiO}_{3-\delta}$ crystals. These magnetic images can be erased by heating the $\text{SrTiO}_{3-\delta}$ crystal above ~ 20 K.

We now present three pieces of new data that further elucidate the underlying nature of the optically induced magnetization in $\text{SrTiO}_{3-\delta}$, and which further support a scenario in which the magnetization arises *not* from collective or long-range interactions, but rather (and more simply) from a metastable spin polarization in the ground states of an ensemble of independent V_{O} -related complexes. We note that V_{O} may be forming defect complexes with residual elemental impurities (for example, Fe) that are present at the tens of parts-per-million level even in nominally pure commercial SrTiO_3 crystals. A detailed analysis of trace impurities in our crystals was presented in our recent work²³.

Figure 4(a) shows optically induced magnetization as a function of temperature for three different $\text{SrTiO}_{3-\delta}$ crystals having V_{O} concentrations that vary over three orders of magnitude. Whether the V_{O} density is large ($6 \times 10^{17} \text{ cm}^{-3}$) or small ($2 \times 10^{14} \text{ cm}^{-3}$), the optically induced magnetization appears at the *same* temperature of about 18 K. If the magnetic moment were due to long-range interactions between V_{O} complexes (for instance, due to itinerant ferromagnetism), then some difference in this critical temperature would be expected as the V_{O} density (and therefore also the electron density n) changes, as was shown for the ferromagnetic semi-

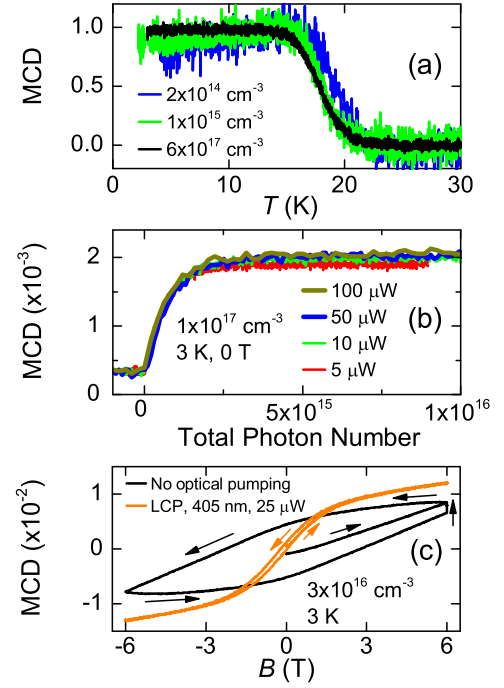


FIG. 4. (a) Temperature-dependent magnetization (as measured by MCD at 425 nm) under continuous pumping with 405 nm LCP light for $\text{SrTiO}_{3-\delta}$ crystals having different V_{O} densities. The curves are normalized in magnitude for comparison. Regardless of the V_{O} concentration, the form of $M(T)$ is the same. (b) Optically induced magnetization in $\text{SrTiO}_{3-\delta}$ as a function of total photon number for different illumination intensities. (c) Magnetization, as measured by MCD at 425 nm, versus magnetic field with (orange curve) and without (black curve) LCP optical pumping. Hysteresis is due to slow magnetization dynamics; faster equilibration occurs when the system is continuously pumped with circularly polarized light.

conductors PbSnMnTe , $\text{Ge}_{1-x}\text{Mn}_x\text{Te}$, or $\text{Ga}_{1-x}\text{Mn}_x\text{As}$ as when the density of itinerant carriers was varied^{28–30}. In contrast, the data in Figure 4(a) are consistent with a single-entity effect, where the polarization of individual V_{O} -related complexes becomes extremely long-lived below 18 K.

Figure 4(b) shows that the build-up and saturation of optically induced magnetization in $\text{SrTiO}_{3-\delta}$ depends only on the total number of photons incident on the sample (at a given wavelength), rather than explicitly on the duration or intensity of illumination. In this data we monitored the temporal build-up of magnetization following illumination with 405 nm light having intensity ranging from 5 μW to 100 μW . Plotting the induced moment as a function of the total number of photons received (rather than as a function of time) collapses all data traces on to a single curve. Again, these data are consistent with a non-interacting ensemble of V_{O} -related complexes that, with some finite cross-section, can become spin-polarized by circularly polarized light. Moreover, these data show that any changes in the background

electron density n due to illumination has little effect.

Finally, Fig. 4(c) shows the measured MCD signal from a $\text{SrTiO}_{3-\delta}$ crystal as a function of applied magnetic field B in the Faraday geometry, for the two cases of continuous optical LCP pumping and no optical pumping. Although it is tempting to associate the observed hysteresis with long-range magnetic order, the observed open hysteresis loops are due to the slow magnetization dynamics that were identified in, for example, Fig. 2. In the absence of optical pumping, the magnetization requires hours to relax and re-equilibrate. With optical pumping, the characteristic timescales are much faster, of order seconds to minutes depending on the illumination intensity. In this latter case, the sample magnetization is better able to remain in approximate equilibrium as the magnetic field is swept at 1 tesla/minute, and the observed hysteresis loop is narrow.

In summary, we developed and used an optically coupled SQUID magnetometer to deliver and monitor circularly polarized light to an *in situ* sample. This

setup was used to investigate the temperature- and time-dependent magnetization in oxygen-deficient $\text{SrTiO}_{3-\delta}$. All data strongly suggest that the optically induced magnetization arises from a long-lived spin polarization in an ensemble of localized and independent V_O -related complexes, rather than from collective effects such as ferromagnetism. We demonstrated the technological promise of persistent optically induced magnetization by optically writing, storing, and optically reading magnetization in a $\text{SrTiO}_{3-\delta}$ crystal in zero magnetic field, pointing to exciting new frontiers in complex oxide electronic and magneto-optical devices.

Acknowledgements

This work was supported by the Los Alamos LDRD program under the auspices of the US DOE, Office of Basic Energy Sciences, Division of Materials Sciences and Engineering. Work at UMN supported in part by NSF under DMR-0804432 and in part by the MRSEC Program of the NSF under DMR-0819885.

-
- ¹ R. Ramesh and D. G. Schlom, MRS Bulletin **33**, 1006 (2008).
 - ² J. Mannhart and D. G. Schlom, Science **327**, 1607 (2010).
 - ³ S. A. Chambers, Adv. Mater. **22**, 219 (2010).
 - ⁴ P. Zubko, S. Gariglio, M. Gabay, P. Ghosez, and J.-M. Triscone, Annu. Rev. Cond. Matter Phys. **2**, 141 (2011).
 - ⁵ H. Y. Hwang, Y. Iwasa, M. Kawasaki, B. Keimer, N. Nagaosa, and Y. Tokura, Nature Mater. **11**, 103 (2012).
 - ⁶ K. A. Müller and H. Burkard, Phys. Rev. B **19**, 3593 (1979).
 - ⁷ C. Lee, J. Destry, and J. L. Brebner, Phys. Rev. B **11**, 2299 (1975).
 - ⁸ B. W. Faughnan, Phys. Rev. B **4**, 3623 (1971).
 - ⁹ R. L. Wild, E. M. Rockar, and J. C. Smith, Phys. Rev. B **8**, 3828 (1973).
 - ¹⁰ A. Brinkman, M. Huijben, M. van Zalk, J. Huijben, U. Zeitler, J. C. Maan, W. G. van der Wiel, G. Rijnders, D. H. A. Blank, and H. Hilgenkamp, Nat. Mater. **6**, 493 (2007).
 - ¹¹ D. A. Dikin, M. Mehta, C. W. Bark, C. M. Folkman, C. B. Eom, and V. Chandrasekhar, Phys. Rev. Lett. **107**, 056802 (2011).
 - ¹² L. Li, C. Richter, J. Mannhart, and R. C. Ashoori, Nat. Phys. **7**, 762 (2011).
 - ¹³ J. A. Bert, B. Kalisky, C. Bell, M. Kim, Y. Hikita, H. Y. Hwang, and K. A. Moler, Nat. Phys. **7**, 767 (2011).
 - ¹⁴ Ariando, X. Wang, G. Baskaran, Z. Q. Liu, J. Huijben, J. B. Yi, A. Annadi, A. R. Barman, A. Rusydi, S. Dhar, et al., Nature Comm. **2**, 188 (2011).
 - ¹⁵ P. Moetakef, J. R. Williams, D. G. Ouellette, A. P. Kajdos, D. Goldhaber-Gordon, S. J. Allen, and S. Stemmer, Phys. Rev. X **2**, 021014 (2012).
 - ¹⁶ J.-S. Lee, Y. W. Xie, H. K. Sato, C. Bell, Y. Hikita, H. Y. Hwang, and C.-C. Kao, Nat. Mater. **12**, 703 (2013).
 - ¹⁷ D. A. Muller, N. Nakagawa, A. Ohtomo, J. L. Grazul, and H. Y. Hwang, Nature **430**, 657 (2004).
 - ¹⁸ J. N. Eckstein, Nature Mater. **6**, 473 (2007).
 - ¹⁹ A. Kalabukhov, R. Gunnarsson, J. Börjesson, E. Olsson, T. Claeson, and D. Winkler, Phys. Rev. B **75**, 121404(R) (2007).
 - ²⁰ J. Shen, H. Lee, R. Valentí, and H. O. Jeschke, Phys. Rev. B **86**, 195119 (2012).
 - ²¹ N. Pavlenko, T. Kopp, E. Y. Tsymbal, G. A. Sawatzky, and J. Mannhart, Phys. Rev. B **85**, 020407(R) (2012).
 - ²² M. Lee, J. R. Williams, S. Zhang, C. D. Frisbie, and D. Goldhaber-Gordon, Phys. Rev. Lett. **107**, 256601 (2011).
 - ²³ W. D. Rice, P. Ambwani, M. Bombeck, J. D. Thompson, G. Haugstad, C. Leighton, and S. A. Crooker, Nature Mater. **13**, 481 (2014).
 - ²⁴ A. Spinelli, M. A. Torija, C. Liu, C. Jan, and C. Leighton, Phys. Rev. B **81**, 155110 (2010).
 - ²⁵ P. J. Stephens, J. Chem. Phys. **52**, 3489 (1970).
 - ²⁶ P. Hosur, A. Kapitulnik, S. A. Kivelson, J. Orenstein, and S. Raghu, Phys. Rev. B **87**, 115116 (2013).
 - ²⁷ D. D. Awschalom, J. Warnock, and S. von Molnár, Phys. Rev. Lett. **58**, 812 (1987).
 - ²⁸ T. Story, R. R. Galazka, R. B. Frankel, and P. A. Wolff, Phys. Rev. Lett. **56**, 777 (1986).
 - ²⁹ Y. Fukuma, H. Asada, M. Arifuku, and T. Koyanagi, Appl. Phys. Lett. **80**, 1013 (2002).
 - ³⁰ S. Koshihara, A. Oiwa, M. Hirasawa, S. Katsumoto, Y. Iye, C. Urano, H. Takagi, and H. Muneoka, Phys. Rev. Lett. **78**, 4617 (1997).